

# Review of the results of the KaoS Collaboration

A. Förster for the KaoS-Collaboration:

I. Böttcher<sup>d</sup>, F. Dohrmann<sup>f</sup>, A. Förster<sup>a,\*</sup>, E. Grosse<sup>f,g</sup>,  
 P. Koczoń<sup>b</sup>, B. Kohlmeier<sup>d</sup>, S. Lang<sup>a</sup>, F. Laue<sup>b,†</sup>,  
 M. Menzel<sup>d</sup>, L. Naumann<sup>f</sup>, H. Oeschler<sup>a</sup>, M. Płoskoń<sup>b</sup>,  
 F. Pühlhofer<sup>d</sup>, W. Scheinast<sup>f</sup>, A. Schmah<sup>a</sup>, T. Schuck<sup>c,‡</sup>,  
 E. Schwab<sup>b</sup>, P. Senger<sup>b</sup>, Y. Shin<sup>c</sup>, H. Ströbele<sup>c</sup>,  
 C. Sturm<sup>a</sup>, F. Uhlig<sup>a</sup>, A. Wagner<sup>f</sup>, W. Waluś<sup>e</sup>

<sup>a</sup> Technische Universität Darmstadt, D-64289 Darmstadt, Germany

<sup>b</sup> Gesellschaft für Schwerionenforschung, D-64291 Darmstadt, Germany

<sup>c</sup> Johann Wolfgang Goethe Universität, D-60325 Frankfurt am Main, Germany

<sup>d</sup> Phillips Universität, D-35037 Marburg, Germany

<sup>e</sup> Uniwersytet Jagielloński, PL-30-059 Kraków, Poland

<sup>f</sup> Forschungszentrum Rossendorf, D-01314 Dresden, Germany

<sup>g</sup> Technische Universität Dresden, D-01062 Dresden, Germany

\* Present address: CERN, CH-1211 Geneva, Switzerland

† Present address: Brookhaven National Laboratory, USA

‡ Present address: MPI für Kernphysik, D-69117 Heidelberg, Germany

E-mail: [Andreas.Foerster@cern.ch](mailto:Andreas.Foerster@cern.ch)

**Abstract.** The production of  $K^+$  and of  $K^-$  mesons in heavy-ion collisions at beam energies of 1 to 2 AGeV has systematically been investigated with the Kaon Spectrometer KaoS. The ratio of the  $K^+$  production excitation function for Au+Au and for C+C reactions increases with decreasing beam energy, which is expected for a soft nuclear equation-of-state. A comprehensive study of the  $K^+$  and of the  $K^-$  emission as a function of the size of the collision system, of the collision centrality, of the kaon energy, and of the polar emission angle has been performed. The  $K^-/K^+$  ratio is found to be nearly constant as a function of the collision centrality and can be explained by the dominance of strangeness exchange. On the other hand the spectral slopes and the polar emission patterns are different for  $K^-$  and for  $K^+$ . Furthermore the azimuthal distribution of the particle emission has been investigated.  $K^+$  mesons and pions are emitted preferentially perpendicular to the reaction plane as well in Au+Au as in Ni+Ni collisions. In contrast for  $K^-$  mesons in Ni+Ni reactions an in-plane flow was observed for the first time at these incident energies.

PACS numbers: 25.75.Dw

## 1. Introduction

Heavy-ion collisions provide the unique possibility to study baryonic matter well above saturation density. The conditions inside the dense reaction zone and the in-medium properties of hadrons can be explored by measuring the particles created in such collisions [1, 2]. In particular, strange mesons are considered to be sensitive to in-medium modifications. Theory predicts a repulsive  $K^+N$  potential and an attractive  $K^-N$  potential in dense matter [3]. At beam energies of 1 to 2 AGeV

strange mesons are produced below or close to their respective threshold in binary nucleon-nucleon collisions ( $NN \rightarrow K^+\Lambda N$  at  $E_{beam} = 1.6$  GeV,  $NN \rightarrow K^+K^-NN$  at  $E_{beam} = 2.5$  GeV). The production at these energies requires multiple nucleon-nucleon collisions or secondary collisions like e.g.  $\pi N \rightarrow K^+Y$  ( $Y = \Lambda, \Sigma$ ) for the  $K^+$  or the strangeness exchange reaction  $\pi Y \rightarrow K^-N$  for the  $K^-$ .  $K^+$  mesons contain an  $\bar{s}$ -quark and hence can hardly be absorbed in hadronic matter consisting almost entirely of u- and d-quarks. The  $K^-$  on the other hand can be reabsorbed via the inverse direction of the strangeness exchange reaction mentioned above.

The experiments were performed with the Kaon Spectrometer (KaoS) at the heavy-ion synchrotron (SIS) at the GSI in Darmstadt [4]. The magnetic spectrometer has a large acceptance in solid angle and in momentum ( $\Omega \approx 30$  msr,  $p_{max}/p_{min} \approx 2$ ). The particle identification and the trigger are based on separate measurements of the momentum and of the time-of-flight. The background due to spurious tracks and pile-up is removed by a trajectory reconstruction based on three large-area multi-wire proportional counters. The short distance of 5 - 6.5 m from the target to the focal plane minimizes the number of kaon-decays in flight. The loss of kaons by decay is accounted for by Monte Carlo simulations using the GEANT code. Three different collision systems have been investigated (Au+Au, Ni+Ni, and C+C) at incident beam energies ranging from 0.6 AGeV to 2.0 AGeV. Results have been published in [5, 6, 7, 8, 9, 10, 11, 12, 13] and will in part be presented in this contribution.

Section 2 briefly summarizes the results on the excitation function of the  $K^+$  production and the conclusions that can be drawn on the nuclear equation-of-state. In section 3 the dependence of the  $K^+$  and of the  $K^-$  production on the collision centrality is discussed. Section 4 shows details on energy spectra and polar angle distributions and in section 5 azimuthal distributions for  $\pi$ ,  $K^+$ , and  $K^-$  are presented.

## 2. $K^+$ production as a probe for the nuclear equation-of-state

Early transport calculations predicted that the  $K^+$  yield in Au+Au collisions at beam energies below the production threshold in nucleon-nucleon collisions would be enhanced by a factor of about 2 if a soft rather than a hard equation-of-state is assumed [1, 14]. Recent calculations take into account modifications of the kaon properties within the dense nuclear medium. The repulsive  $K^+N$  potential assumed depends nearly (or less than) linearly on the baryonic density [3] and thus reduces the  $K^+$  yield accordingly. On the other hand, at subthreshold beam energies the  $K^+$  mesons are created in secondary collisions involving two or more particles and hence their production depends at least quadratically on the density. To disentangle these two competing effects we have studied the  $K^+$  production in a light (C+C) and in a heavy collision system (Au+Au) at different beam energies near threshold. The maximum baryonic density reached in Au+Au reactions is significantly higher than in C+C reactions. Moreover, the maximum baryonic density reached in Au+Au reactions depends strongly on the compression modulus of nuclear matter  $\kappa$  [15, 14] whereas in C+C collisions this dependence is rather weak [16]. Hence, the ratio of the  $K^+$  multiplicity per nucleon  $M/A$  in Au+Au to the one in C+C is expected to be sensitive to the compression modulus  $\kappa$  while providing the advantage that uncertainties within the experimental data (beam normalization etc.) and within the transport model calculations (elementary cross sections etc.) are partly cancelled.

Figure 1 shows a comparison of the ratio  $(M/A)_{Au+Au}/(M/A)_{C+C}$  for  $K^+$  together with the predictions of RQMD transport model calculations [16]. The

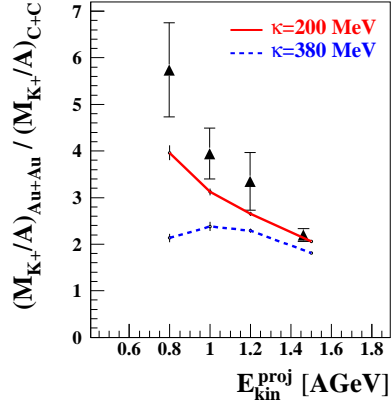


**Figure 1.** The ratio of the  $K^+$  multiplicity per nucleon  $M/A$  in Au+Au to the one in C+C reactions as a function of the beam energy for inclusive reactions. The data are compared to the results of RQMD transport model calculations [16]. The calculations were performed with two different values for the compression modulus:  $\kappa = 200$  MeV (a “soft” equation-of-state), denoted by the solid line, and  $\kappa = 380$  MeV (a “hard” EoS), indicated by the dashed line.

calculations were performed with two values for the compression modulus:  $\kappa = 200$  MeV (solid line) and  $\kappa = 380$  MeV (dashed line) corresponding to a “soft” or to a “hard” nuclear equation-of-state, respectively. The RQMD transport model takes into account a repulsive  $K^+N$ -potential and uses momentum-dependent Skyrme forces to determine the compressional energy per nucleon (i.e. the energy stored in the compression). The comparison demonstrates clearly that only the calculation based on a soft nuclear equation-of-state reproduces the trend of the experimental data. A similar result is obtained using the transport code IQMD [17].

### 3. The centrality dependence

The centrality of the collision was derived from the multiplicity of charged particles measured in the interval  $12^\circ < \theta_{lab} < 48^\circ$  by a hodoscope consisting of 84 plastic-scintillator modules. In order to study the centrality dependence the data measured close to midrapidity ( $\theta_{lab} = 40^\circ$ ) were grouped into five centrality bins both for Ni+Ni and for Au+Au collisions at 1.5 AGeV.

The inclusive kaon multiplicity for each centrality bin is defined as  $M = \sigma_K / (f \cdot \sigma_R)$  with  $\sigma_K$  being the kaon production cross section and  $(f \cdot \sigma_r)$  being the fraction of the reaction cross-section for the particular event class which was determined by normalising the charged particle multiplicity distribution measured with a minimum bias trigger. The corresponding mean number of participating nucleons for each centrality bin  $A_{part}$  was calculated from the measured reaction cross-section fraction for this bin using a Glauber model.

Figure 2 presents the multiplicity per number of participating nucleons  $M/A_{part}$  as a function of  $A_{part}$  for  $K^+$ , for  $K^-$ , and for pions. The lines are functions  $M \propto A_{part}^\alpha$  fitted to the data yielding similar values of  $\alpha \approx 1.2 - 1.3$  for  $K^+$  and for  $K^-$  as well in

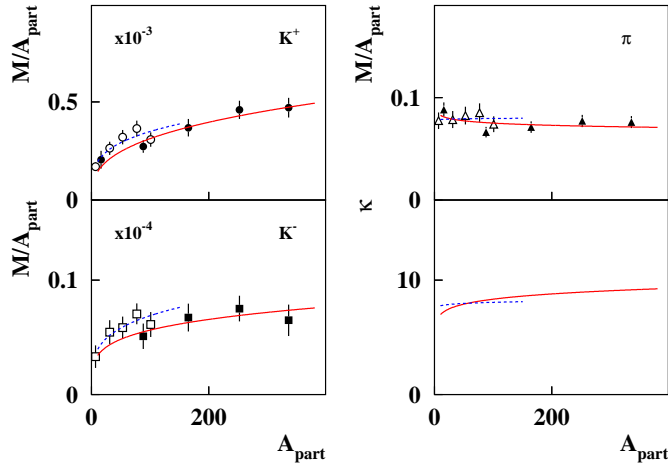


**Figure 2.** Particle yields  $M$  per participant  $A_{part}$  as a function of  $A_{part}$  obtained from Ni+Ni (open symbols) and Au+Au collisions (full symbols) at 1.5 GeV. The lines are functions  $M \propto A_{part}^\alpha$  fitted to the data (solid lines for Au+Au, dashed lines for Ni+Ni collisions) with  $\alpha \approx 1.2 - 1.3$ . The lower right panel shows the resulting values of the equilibration constant  $\kappa$  for the strangeness exchange reaction (see text) as determined from the fits shown above [18]. The data are taken around midrapidity and extrapolated to  $4\pi$  [12].

Au+Au as in Ni+Ni and  $\alpha \approx 1.0$  for pions. The resulting  $K^-/K^+$  ratio is about 0.02 for Au+Au as well as for Ni+Ni and is rather constant as a function of the collision centrality.

At low incident energies the strangeness-exchange reaction  $\pi + Y \rightleftharpoons K^- + N$  plays a key role in the  $K^-$  production. If the rates for the  $K^-$  production are equal to those for the  $K^-$  absorption, this reaction is in chemical equilibrium. In this case the law-of-mass action is applicable and leads to the following relation between particle yields  $[\pi] \cdot [Y]/[K^-] \cdot [N] = \kappa$  with  $[x]$  being the multiplicity of particle  $x$  and  $\kappa$  the equilibration constant [18, 21]. At this low beam energies the hyperons are produced together with  $K^+$  and  $K^0$  in equal rates, hence,  $[Y] = [K^+] + [K^0] \approx 2 \cdot [K^+]$ . The multiplicity of nucleons  $[N]$  can be related to the average number of participants  $A_{part}$ . The pion density  $[\pi]$  contains unequal contributions from  $[\pi^+]$ ,  $[\pi^0]$  and  $[\pi^-]$  due to the isospin asymmetry of the colliding system. The details of the calculation to obtain the equilibration constant  $\kappa$  from the measured data can be found in [18]. The results using the separate fits to the Au+Au and Ni+Ni data are presented in the lower right panel of figure 2 and they show that  $\kappa$  is independent of the centrality and of the collision system within the experimental uncertainties.

#### 4. Energy spectra and polar angle distributions

Although the production of  $K^+$  and of  $K^-$  mesons is strongly coupled via the strangeness exchange reaction significant differences between  $K^+$  and  $K^-$  have been found [12].

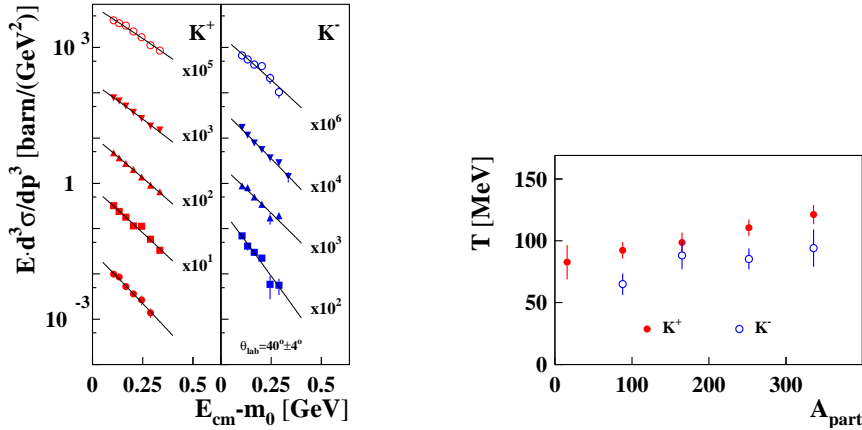


**Figure 3.** Left: Invariant cross sections for  $K^+$  and for  $K^-$  in Au+Au collisions at  $E_{beam} = 1.5$  AGeV for the different centrality bins. The open circles depict the most central data, the other bins are shown from the top to the bottom of the figure with decreasing centrality. Right: Inverse slope parameters  $T$  as a function of the number of participating nucleons  $A_{part}$  for  $K^+$  (full symbols) and  $K^-$  (open symbols).

The left hand side of figure 3 shows the production cross sections for  $K^+$  and for  $K^-$  mesons measured close to midrapidity as a function of the kinetic energy in the center-of-momentum system for the five centrality bins in Au+Au collisions at 1.5 AGeV. The uppermost spectra correspond to the most central reactions, the subsequent bins are shown from the top to the bottom of the figure with decreasing centrality. The error bars represent the statistical uncertainties of the kaon and the background events. An overall systematic error of 10% due to efficiency corrections and beam normalization has to be added. The solid lines represent the Boltzmann function  $d^3\sigma/dp^3 = C \cdot E \cdot \exp(-E/T)$  fitted to the data.  $C$  is a normalization constant and the exponential function describes the energy distribution with  $T$  being the inverse slope parameter.

The spectra presented in figure 3 exhibit a distinct difference between  $K^-$  and  $K^+$ : The slopes of the  $K^-$  spectra are steeper than those of the  $K^+$  spectra. The inverse slope parameters  $T$  as a function of  $A_{part}$  for each centrality bin are displayed in the right hand side of the figure.  $T$  increases with increasing centrality and is found to be significantly lower for  $K^-$  than for  $K^+$ , even for the most central collisions. The same behaviour has been observed for Ni+Ni collisions at 1.93 AGeV.

Another observable showing a distinct difference between  $K^+$  and  $K^-$  is the polar angle emission pattern. Due to limited statistics we considered only Au+Au collisions at 1.5 AGeV grouped into two centrality bins: near-central (impact parameter  $b < 6$  fm) and non-central collisions ( $b > 6$  fm) [12]. Figure 4 displays the polar angle distribution for  $K^+$  (upper panels) and for  $K^-$  (lower panels), both for near-central (right) and for non-central collisions (left).

The solid lines represent the function  $1 + a_2 \cdot \cos^2(\theta_{cm})$  which is fitted to the experimental distributions with the values of  $a_2$  given in the figure. In near-central collisions the  $K^-$  mesons exhibit an isotropic emission pattern whereas the emission

of the  $K^+$  mesons is forward-backward peaked. The angular distributions observed for  $K^+$  and for  $K^-$  in Ni+Ni collisions at 1.93 AGeV are similar to the ones presented in figure 4 [10].

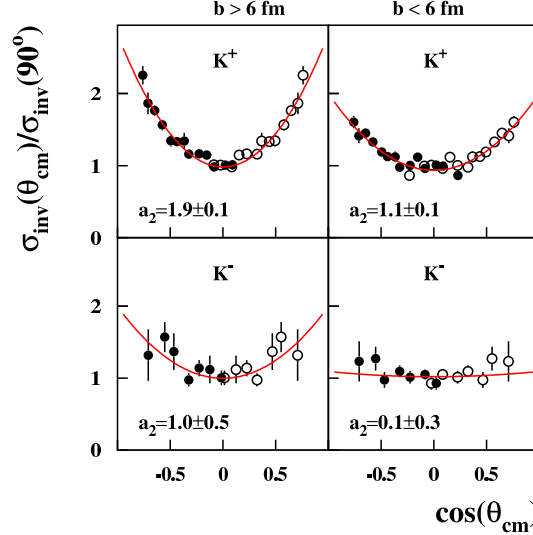


**Figure 4.** Polar angle distributions for  $K^+$  (upper panels) and for  $K^-$  (lower panels) in Au+Au collisions at  $E_{beam} = 1.5$  AGeV. The left panels show data for impact parameters  $b > 6$  fm, the right ones for  $b < 6$  fm. The fits and the parameter  $a_2$  are as described in the text.

## 5. The azimuthal distribution of the $K^+$ - and of the $K^-$ -emission

The left hand side of figure 5 shows the azimuthal distributions of  $\pi^+$  and  $K^+$  mesons for semi-central Au+Au collisions at 1.5 AGeV, the right hand side the distributions for  $\pi^+$ ,  $K^+$  and  $K^-$  in Ni+Ni collisions at 1.93 AGeV [13]. The distributions are corrected for the angular resolution of the reaction plane determination [19]. The data are fitted using the first two components of a Fourier series  $dN/d\Phi \sim 2v_1 \cos(\phi) + 2v_2 \cos(2\phi)$  resulting in values for  $v_1$  and  $v_2$  as given in the figures together with the statistical errors. The determination of the coefficient  $v_1$  is subject to an additional systematic error of 0.04.

In Au+Au both,  $\pi^+$  and  $K^+$  mesons, exhibit a pronounced enhancement at  $\phi = \pm 90^\circ$ , i.e. perpendicular to the reaction plane. For  $\pi^+$  mesons this effect can be interpreted as rescattering and absorption within the spectator fragments.

The study of Ni+Ni collisions was performed at a higher incident energy of 1.93 AGeV. The resulting higher production cross section for  $K^-$  mesons provides an opportunity to study both charged kaon species. The data are shown on the right hand side of figure 5 along with  $\pi^+$  mesons for semi-central collisions. Both,  $\pi^+$  and  $K^+$  mesons follow, the same trend already observed in Au+Au collisions. The values for  $v_2$  are smaller than in Au+Au as one might expect for the smaller system. In contrast to the  $\pi^+$  and to the  $K^+$  mesons the  $K^-$  mesons show an in-plane enhancement.

This “positive” (in-plane) elliptic flow of particles is observed for the first time in heavy-ion collisions at SIS energies. In contrast to this observation one would expect

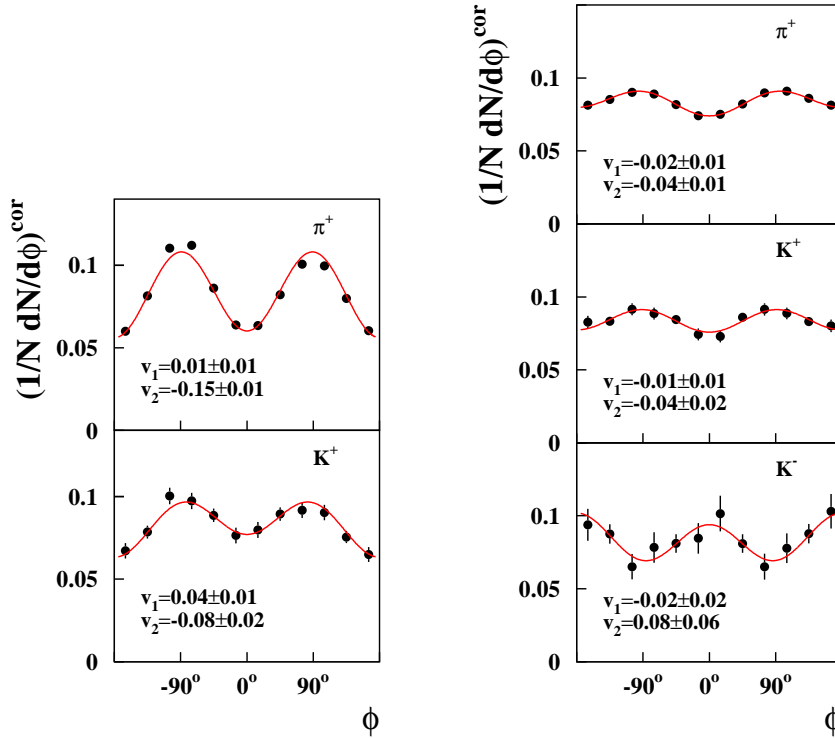


**Figure 5.** Left: Azimuthal distributions of  $\pi^+$  and of  $K^+$  mesons for semi-central Au+Au collisions at 1.5 AGeV. The data are corrected for the resolution of the reaction plane and refer to impact parameters of  $5.9 \text{ fm} < b < 10.2 \text{ fm}$ , rapidities of  $0.3 < y/y_{beam} < 0.7$  and momenta of  $0.2 \text{ GeV} < p_t < 0.8 \text{ GeV}$ . The lines are fits as described in the text. Right: Azimuthal distributions of  $\pi^+$ , of  $K^+$  and of  $K^-$  mesons for semi-central Ni+Ni collisions at 1.93 AGeV. The data refer to impact parameters of  $3.8 \text{ fm} < b < 6.5 \text{ fm}$  and the same range in rapidity and  $p_t$  as the Au+Au data.

a preferential out-of-plane emission (negative elliptic flow) of  $K^-$  mesons due to their large absorption cross section in spectator matter.

A depletion of the expected out-of-plane emission pattern of  $K^-$  mesons might be due to the fact that they are produced via strangeness-exchange reactions. This causes a delay in the freeze-out of the  $K^-$  mesons [12, 20, 21] and, hence, a reduced shadowing effect by the spectator fragments which have moved further away. The observed in-plane emission of  $K^-$  mesons, however, cannot be easily explained by this scenario.

In order to quantitatively explain the  $K^+$  and  $K^-$  meson azimuthal distributions in figure 6 we compare our data to recent results of the IQMD model [22]. This transport calculation takes into account both the space-time evolution of the reaction system and the in-medium properties of the strange mesons. The dashed and solid lines represent results of calculations without and with in-medium potentials, respectively. In the case of the  $K^+$  mesons the effect of the repulsive  $K^+N$  potential is small in this model. A large fraction of the observed out-of-plane enhancement, in contrast to other

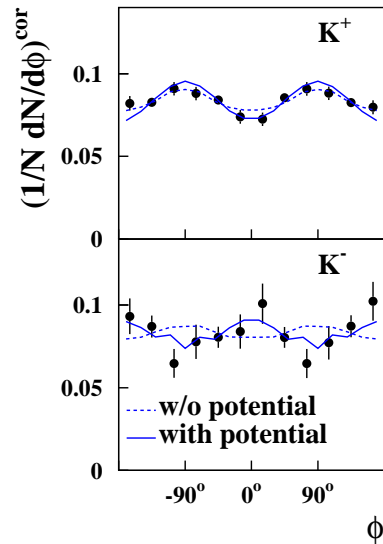


**Figure 6.** Comparison of the data from Ni+Ni reactions at 1.93 AGeV (see fig. 5) with IQMD model calculations [22].

models [23, 24, 25], is caused by the scattering of  $K^+$  mesons. The transport code (HSD) [25] in contrast predicts a dominant influence of the potential on the emission pattern of the  $K^+$  mesons. In the system Au+Au at 1 AGeV where both size and life time of the fireball are larger than in the Ni+Ni case, the effect of the repulsive  $K^+$ N potential was found to be very important [8, 23, 24].

The lower part of figure 6 shows a comparison of the  $K^-$  data to calculations without (dashed) and with (solid)  $K^-$ N potential. When neglecting the  $K^-$ N potential, the calculation predicts a weak out-of-plane elliptic flow caused by shadowing. This effect is rather small because of the late emission of  $K^-$  mesons. When taking into account the attractive in-medium  $K^-$ N potential the model is able to describe the experimental in-plane elliptic flow pattern much better. Model calculations with the HSD code [25] predict a flat azimuthal distribution both with and without a  $K^-$ N potential and, hence cannot explain the observed in-plane flow of  $K^-$  mesons.

## References

- [1] J. Aichelin and C. M. Ko, Phys. Rev. Lett. **55** (1985) 2661.
- [2] G. Q. Li, C. H. Lee and G. E. Brown, Phys. Rev. Lett. **79** (1997) 5214.
- [3] J. Schaffner-Bielich, J. Bondorf, I. N. Mishustin, Nucl. Phys. **A 625** (1997) 325.
- [4] P. Senger et al. (KaoS), Nucl. Instr. Meth. **A 327** (1993) 393.
- [5] D. Miśkowiec et al. (KaoS), Phys. Rev. Lett. **72** (1994) 3650.
- [6] W. Ahner et al. (KaoS), Phys. Lett. **B 393** (1997) 31.
- [7] R. Barth et al. (KaoS), Phys. Rev. Lett. **78** (1997) 4007.
- [8] Y. Shin et al. (KaoS), Phys. Rev. Lett. **81** (1998) 1576.



- [9] F. Laue, C. Sturm et al. (KaoS), Phys. Rev. Lett. **82** (1999) 1640.
- [10] M. Menzel et al. (KaoS), Phys. Lett. **B495** (2000) 26.
- [11] C. Sturm et al. (KaoS), Phys. Rev. Lett. **86** (2001) 39.
- [12] A. Förster, F. Uhlig et al. (KaoS), Phys. Rev. Lett. **91** (2003) 152301.
- [13] F. Uhlig, A. Förster et al. (KaoS), submitted to Phys. Rev. Lett., nucl-ex/0411021.
- [14] G.Q. Li and C.M. Ko, Phys. Rev. **C 54** (1996) R2159.
- [15] J. Aichelin, Phys. Rep. **202** (1991) 233.
- [16] C. Fuchs et al., Phys. Rev. Lett. **86** (2001) 1974.
- [17] C. Hartnack and J. Aichelin, J. Phys. G **28** (2002) 1649.
- [18] J. Cleymans, A. Förster, H. Oeschler, K. Redlich, F. Uhlig, Phys. Lett. **B 603** (2004) 146.
- [19] D. Brill et al. (KaoS), Z. Phys. **A 355** (1996) 61.
- [20] C. Hartnack, H. Oeschler, J. Aichelin, Phys. Rev. Lett. **90** (2003) 102302; Phys. Rev. Lett. **94** (2004) 149903.
- [21] H. Oeschler, J. Phys. G **27** (2001) 257.
- [22] C. Hartnack et al., Eur. Phys. J. **A 1** (1998) 151 and to be published.
- [23] Z.S. Wang, C.Fuchs, A. Faessler, T. Gross-Boelting, Eur. Phys. J. **A 5** (1999) 275.
- [24] G. Q. Li et al., Phys. Lett. **B 381** (1996) 17.
- [25] A. Mishra, E. Bratkovskaya, J. Schaffner-Bielich, S. Schramm, H. Stöcker, Phys. Rev. **C 70** (2004) 044904.